Journal of Muscle Research and Cell Motility (2025) 46:407–414
https://doi.org/10.1007/s10974-025-09712-z

ORIGINAL PAPER

Direct measurement of mavacamten and deoxyATP perturbation of the SRX/DRX ratio in porcine cardiac myofibrils using a simple, accessible and multiplexed approach

Matvey Pilagov[1] · Ateeqa Naim[1] · Kenneth S. Campbell[2] · Thomas Kampourakis[2] · Michael A. Geeves[1] · Neil M. Kad[1]

Received: 25 July 2025 / Accepted: 26 September 2025 / Published online: 22 October 2025

Abstract
Cardiac muscle adapts to varying physiological demands by modulating the number of active myosin II motors available for contraction. These motors are organized into thick filaments in the sarcomere and generate force through an ATP-dependent interaction with thin filaments that contain actin. To conserve energy, when demand is low myosin can occupy the super-relaxed (SRX) state, which acts as a reserve. Here, we build upon the earlier studies to quantify the size of this cardiac reserve using fluorescence imaging of Cy3-ATP directly in myofibrils. This approach employs a pulse-chase method and exploits the high permeability of isolated myofibrils to monitor nucleotide release in situ. By preserving sarcomeric architecture while enabling rapid reagent exchange, this method bridges the gap between complex single-molecule imaging and traditional stopped-flow bulk assays using MANT-ATP. Using this approach we have studied biochemical perturbation of the SRX reserve with deoxyATP and mavacamten. DeoxyATP caused large depletion of the cardiac reserve, and mavacamten increased its size, consistent with its clinical application. Our results demonstrate the utility of this technique and the potential for further enhancement using multiplexing (i.e. imaging multiple samples in the same acquisition period), holding promise for future applications in health and disease.

Keywords Fluorescence microscopy · Cardiac reserve · Myotropes · Thick filament regulation · Energyconservation · Sarcomere Physiology

Introduction

Cardiac muscle continuously contracts and relaxes over the lifetime of all higher animals. It is organised into sarcomeres comprised of lateral arrays of thick filaments each one with ~300 myosin motors capable of generating force. However, the number of motors available for cardiac contraction is modulated according to the prevailing conditions, thus optimizing energy usage. Examples of dynamic changes requiring greater numbers of available myosins include β-adrenergic stimulation or raised afterload due to elevated systemic blood pressure. These regulated motors form a reserve pool of myosins and the molecular mechanisms that lead to this regulation are currently under intense investigation.

Controlling the number of available myosins allows the heart to adapt to inotropic stresses by recruiting more myosins to pump harder and faster, or when demands are low, to rest myosins. An early and important observation is that myosin heads in muscle consume ATP~five-times slower than myosin heads in solution (Ferenczi et al. 1978). This suggests that the sarcomeric architecture may play a role in controlling energy consumption (Starr and Offer 1978; Cooke 2011). In this study, we offer a method to rapidly and directly estimate the amounts of active myosins in the near-native environment of muscle myofibrils.

Contraction in muscle occurs in myofibrils, long linear arrays of sarcomeres, and is generated by the double-headed motor myosin II, which forms helically arrayed 'thick' filaments packed hexagonally in three dimensions.

✉ Neil M. Kad
n.kad@kent.ac.uk

[1] School of Biosciences, University of Kent, Canterbury, Kent, UK

[2] Division of Cardiovascular Medicine, University of Kentucky, Lexington, KY, USA

Between every three thick filaments is a thin filament that is formed from actin and decorated with tropomyosin and troponin, which control access of myosin to actin (Gordon et al. 2000). Access is gated by calcium binding to the control protein troponin (subunit C), which leads to azimuthal movement of tropomyosin across the thin filament to expose myosin binding sites on actin (McKillop and Geeves 1993; Poole et al. 2006); and is cooperatively propagated along the thin filament (Fraser and Marston 1995; Conibear and Geeves 1998; Desai et al. 2015). When myosin hydrolyses ATP to ADP.Pi it can then bind to actin, which stimulates the release of Pi and ADP coupled to the myosin working stroke, leading to force generation and muscle shortening. Binding of a subsequent ATP molecule detaches myosin, and its hydrolysis allows the head to recover for the next cycle (Lymn and Taylor 1971). The number of available myosins governs the force generated (Spudich 2019), and amount of ATP consumed. Therefore, control of myosin availability is paramount in balancing the energy demands of muscle.

Relatively recently, in a field that has a very long history, a new biochemical state of myosin was identified by the Cooke lab, first in skeletal (Stewart et al. 2010) and then in cardiac muscle (Hooijman et al. 2011). Using a pulse-chase approach where MANT-ATP was perfused into relaxed permeabilized muscle fibres before rapid dilution with unlabelled ATP, a bi-phasic fluorescence decay was observed by fluorescence microscopy, corresponding to the release of MANT-ADP. The faster phase was in part attributed to the normally relaxed turnover of ATP by myosin (DRX state; not activated by actin binding) and the second slower phase(s) was termed the super-relaxed state (SRX). This state potentially solves the energy paradox by acting as a reserve of myosins to be called upon when needed. It is also possible that a subset of the SRX is represented by a structural folded state termed the interacting heads motif (IHM) however discussion over this is hotly debated and lies outside the scope of this article (for a review see (Craig and Padron 2022). Over the subsequent years ubiquitous use of a version of this MANT-ATP assay was employed to identify the presence of the SRX state. However, the assay used a spectrophotometric approach that relied on the change in fluorescence of MANT-ATP upon binding to myosin (Hiratsuka 1983; Cremo et al. 1990; Woodward et al. 1991; Myburgh et al. 1995). These assays have also been used beyond myofilaments to reveal two phases in stopped-flow measurements of MANT-ADP release for purified/recombinant myosins (Anderson et al. 2018; Gollapudi et al. 2021). However, the use of the MANT-ADP release assay was cast into doubt because the existence of two phases that are in rapid equilibrium would produce only a single phase as discovered in more recent studies of HMM and isolated myosin (Mohran et al. 2024; Cail et al. 2025). However the use of MANT-ATP with myofibrils has shown that two phases can exist, suggesting the milieu of the myofibril may contribute to the separation of the two species (Walklate et al. 2022; Mohran et al. 2024). This uncertainty in the field requires a unifying approach.

We and others developed a new single molecule imaging assay to measure the binding and release of fluorescent ATP in the milieu of myofibrils (Nelson et al. 2020; Pilagov et al. 2023). These preparations are ideal for studying myosin activity because they preserve the sarcomeric structure while also being small enough to minimize diffusion times. This latter point is of concern, since rate constants of nucleotide release will be sensitive to permeability. The highly permeable nature of myofibrils has long been established (Stehle et al. 2009) with solution exchange on the sub-ms timescale (Solzin et al. 2007). However, although these single molecule techniques provide very detailed information on the spatial location of myosin activity, they are also very complex and time-consuming. Therefore, a middle ground technique is needed. To bridge this gap, we present an approach here to measure the activity of myosins in myofibrils directly using bulk fluorescence imaging. This technique uses a pulse-chase approach based on that of the Cooke lab (Hooijman et al. 2011), but with the very high permeability of myofibrils, and using Cy3-ATP instead of MANT-ATP.

Results and discussion

Figure 1a shows an overview of the approach, myofibrils from porcine cardiac left ventricular tissue are immobilised on a coverslip surface and incubated with 1 μM Cy3-ATP (in this study Cy3-ATP is a mixture of 2' and 3' attachments to the ribose (Toseland and Webb 2011)) with 500 μM unlabelled ATP to ensure relaxed conditions for 30 min before performing a rapid wash step, which clears out the fluorescent ATP and washes in 5 mM unlabelled ATP. Following this step images of each myofibril were taken for 15 ms every 5 s, and the laser illumination terminated between images to eliminate photobleaching. During the dark period we move the stage to visualize up to three more myofibrils in the imaging chamber before returning to the first. To achieve this, we built our own proof-of-concept stage system with Arduino controllers to coordinate with laser flashes, however commercial automation would reduce the dead-time between images and increase multiplexing. We continued to take images for 30 min and then during post-imaging we select a region of the myofibril that does not include any edges using FIJI (ImageJ, NIH). The fluorescence intensity in this region is projected through time to

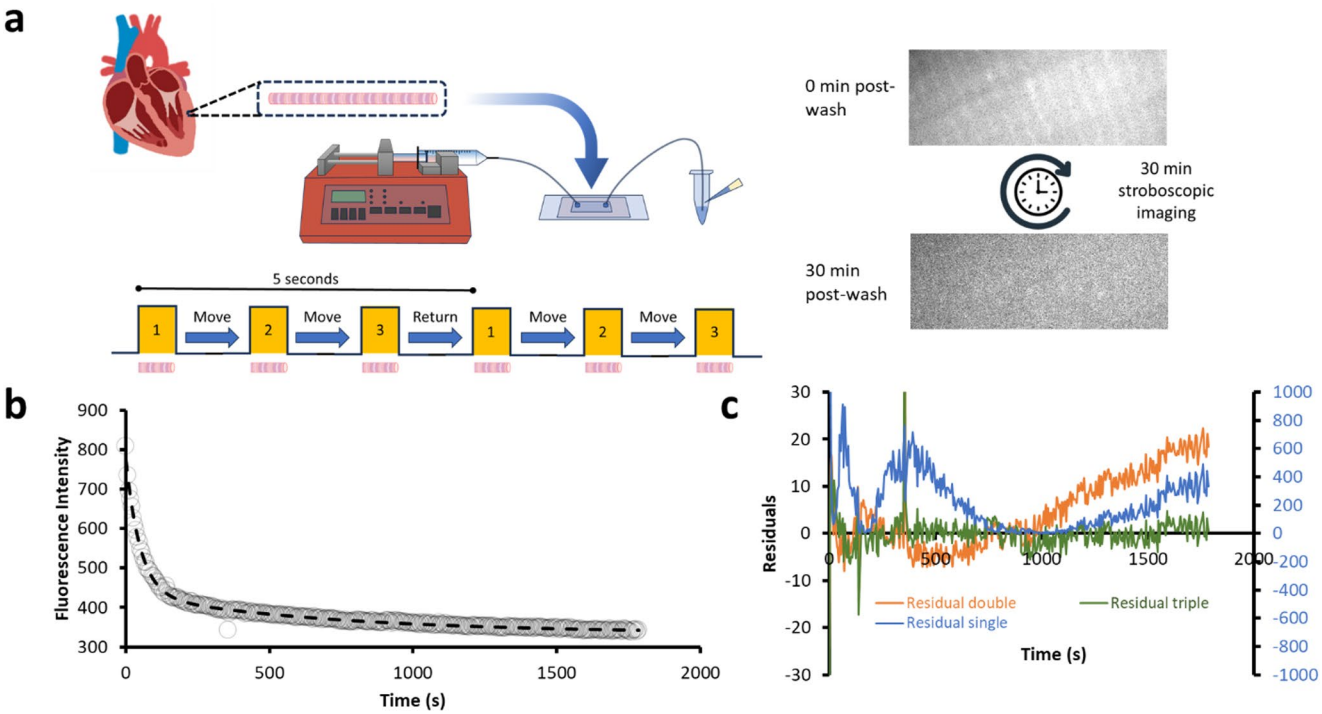

Fig. 1 Overview of the method for rapid multiplexed imaging of myofibrils. (**a**) Myofibrils are purified from left ventricular cardiac trabeculae and then injected into a microfluidic cell. After wash-in and then wash-out of Cy3-ATP, the bulk fluorescence over the myofibril is measured and shows a decay over the 30-minute imaging period. (**b**) The fluorescence decay is best fitted as shown to a triple exponential. This is determined by examination of the (**c**) residuals shown for single (blue), double (orange) and triple (green) exponential fits. The single exponential fit residuals are plotted against the right Y-axis showing the large differences from the data. For the double and triple exponentials, these are plotted against the left Y-axis scale. The triple exponential fit (green) is preferred because it shows a better fit throughout the time range particularly at the longer time periods where it is important to obtain a good fit. All data were fit using a logarithmic weighting (due to their exponential distribution), therefore the residuals do not average on zero as would be expected from linear weighting

produce a transient of nucleotide release (Fig. 1b). The transient is best fit to either a double or triple exponential decay, determined by examination of the amplitude and systematic noise of the residuals for each fit (Fig. 1c). The fastest phase ($>0.041\ s^{-1}$) is likely due to remnants of the Cy3-ATP washout, actin-induced ADP release, and/or non-specific binding of nucleotide (Amrute-Nayak et al. 2014; Ušaj et al. 2021) and so is ignored for the remainder of the analysis. However, the remaining two phases fall into the rate constant regime consistent with the DRX ($0.041 > 0.007\ s^{-1}$) and SRX ($<0.007\ s^{-1}$) states of myofibrils (Cooke 2011; Walklate et al. 2022). Figure 2a shows how these rate boundaries were objectively determined. The rate versus percent population of the two slower phases is plotted for every untreated myofibril studied (filled black circles) and then fitted to a Gaussian mixtures model, which uses a statistical approach to cluster datapoints together. This creates a probability density around the cluster point shown as coloured contours in Fig. 2a (yellow at peak, blue towards edges). By defining the boundary at 99.95% between populations (Fig. 2a: black contour line) an equal number of rate constants in both the DRX and SRX regimes are seen for the untreated data. The average rate constant for DRX and SRX was $0.021\ s^{-1} \pm 0.002$ and $0.0021\ s^{-1} \pm 0.0005$ (errors are SEM, $n=10$ myofibrils) respectively using this approach. It could be argued that the latter rate constant is due to photobleaching; however, this still indicates there is a second distinctly slower species. Furthermore, our recent unpublished study (Mohran et al. 2025) shows that using this technique we can detect Cy3-ADP release rates > 10-fold slower than those observed here. Together, these observations indicate that the slower rate constant is unaffected by photobleaching.

To test that the two rate constants reflect the two populations of SRX and DRX we perturbed the DRX/SRX ratio by washing out the Cy3-ATP with a solution containing (1) 30 µM mavacamten + 5mM unlabelled ATP or (2) 100% (5 mM) deoxyATP. These were chosen because they provide the expected lower (mavacamten) and upper (dATP) limits on the amount of DRX. Mavacamten has been shown to reduce activity in purified myosin (Anderson et al. 2018), myofibrils (Walklate et al. 2022), and patients (Zampieri et al. 2021). It is the only myotropic drug to receive FDA-approval for the treatment of the cardiac condition obstructive hypertrophic cardiomyopathy. Conversely, dATP has been shown extensively to activate purified myosin, muscle fibres and myofibrils (Regnier et al. 2000; Walklate et al.

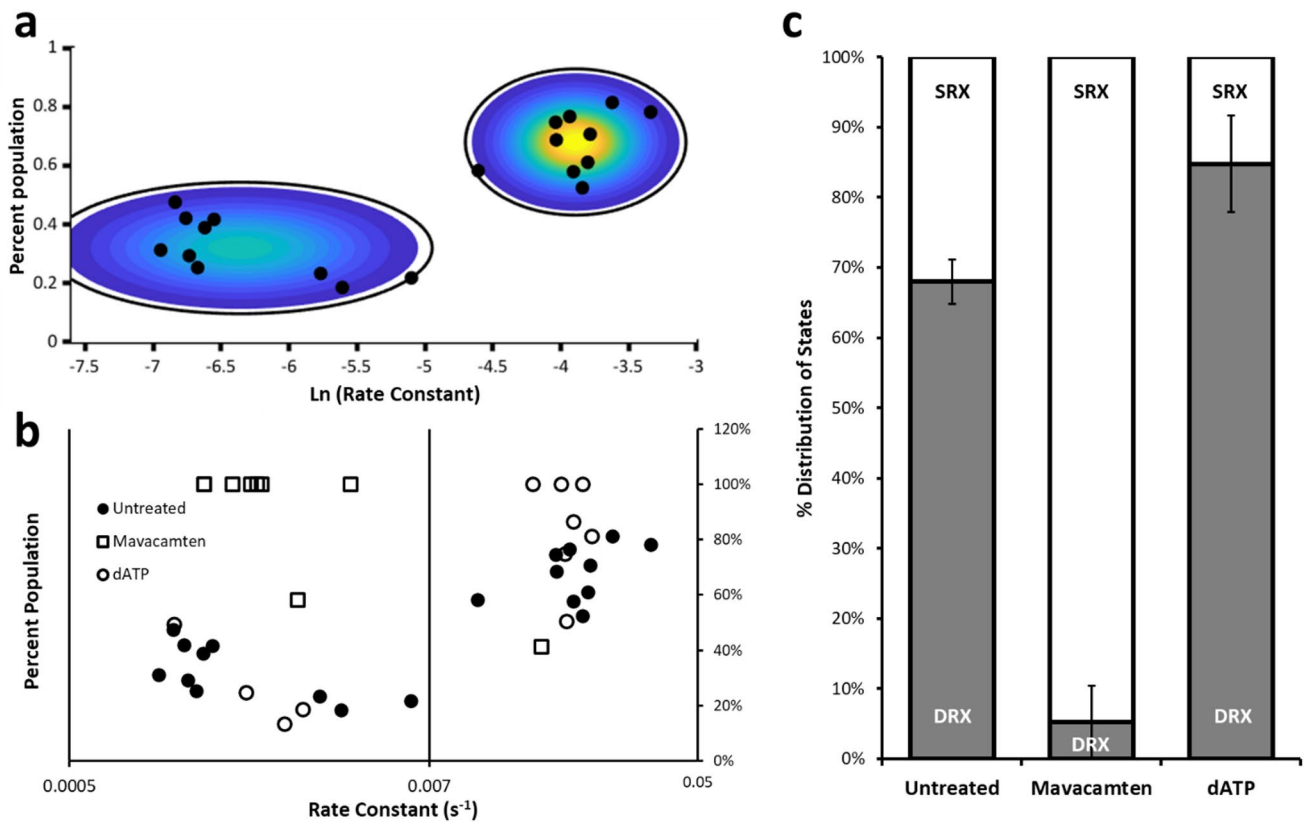

Fig. 2 Perturbing the DRX/SRX ratio using mavacamten and dATP. (**a**) Untreated data fitted to a Gaussian mixtures model shows two major populations. The colour distribution reflects the probability density of the 2D Gaussian used for fitting and the surrounding black circle is the density at 99.95% probability; this was used to independently define the boundaries between the populations for the SRX vs. DRX populations. (**b**) Rate constants for all myofibrils are plotted versus their percent amplitude (taking only the slower two phases of the transients (see Fig. 1b)). Values with only a single population are marked at 100%. This representation provides an overview of all the data, showing untreated (filled circles), treated with 30 μM mavacamten (squares) and 100% dATP (open circles). The vertical line in the graph represents the boundary rate constant defined by the Gaussian mixtures model. For clarity, (a) and (b) are aligned. (**c**) Provides a percentage of the DRX/SRX populations determined from the fitted data for each myofibril averaged across all measured myofibrils. This chart shows relative to DRX in untreated 68.0% (±3.2 SEM $n=10$ myofibrils) there is a significant decrease ($p<0.002$; Student's T-test) in the presence of mavacamten to 5.2% (±5.2 SEM $n=8$ myofibrils). With deoxyATP (dATP), the total amount of DRX is significantly increased ($p<0.05$; Student's T-test) to 94.8% (±8.0 SEM $n=7$ myofibrils)

2022; Mohran et al. 2024). In many of the cases with these myotropes we observed only one of the two slower phases (DRX or SRX) indicating a full shift in distribution of the population for that myofibril. Plotting the observed populations as we did for untreated revealed again two clear populations for dATP treated myofibrils (Fig. 2b open circles) with average rate constant per regime DRX = 0.020 s^{-1} (±0.001 SEM $n=7$ observations), and SRX = 0.002 s^{-1} (±0.003 SEM $n=4$ observations), three of the seven measured samples had only DRX with no apparent SRX population (plotted as 100% DRX). Overall, this resulted in an elevated percentage population in DRX relative to untreated (Fig. 2c). By contrast, mavacamten treatment showed only a single instance of a myofibril with a rate constant that fell into the DRX category (rate constant = 0.016 s^{-1}). The remainder were entirely SRX leading to a large overall shift towards SRX (Fig. 2c) with an average rate constant = 0.002 s^{-1} (±0.0003 SEM $n=8$ observations). This is expected at the saturating concentrations of mavacamten used and does not indicate if there would be intermediate rate populations as suggested from stopped-flow experiments (Mohran et al. 2024). However, given that the SRX rate constant is the same with and without mavacamten, this suggests that the drug may work by shifting the population of myosin ATPases to a defined SRX state. To quantitate the amount of DRX, we determined the amplitudes of the transients per myofibril and then plotted these as an average across all myofibrils studied (Fig. 2c). These data show that untreated porcine myofibrils possess 68.0% DRX, whereas upon treatment with a vast excess over Kd quantity of mavacamten, the DRX population drops significantly to 5.2% and with dATP there was an increase in DRX to 84.8% (errors in Fig. 2 legend). These results are in close agreement with previously published data for the effects on porcine myofibrils (Walklate et al.

2022; Pilagov et al. 2024), indicating this method provides straightforward analysis across the full range of DRX proportions measured to date.

Conclusions

We show here that it is possible to image the fluorescence decay following a rapid washout of Cy3-ATP to detect at least two phases in cardiac myofibrils. This approach builds on the pioneering work from the Cooke lab and offers a fast, reliable way to make measurements of the cardiac myosin reserve within the myofilament lattice. Cy3-ATP provides a strong fluorescence signal that does not affect the activity of myosin (Conibear et al. 1996; Amrute-Nayak et al. 2014; Ušaj et al. 2021), and the use of myofibrils ensures the myofilament lattice structure but with the advantage rapid diffusion necessary for chase experiments. Furthermore, our method utilizes rapid flashes of the excitation laser with a dark period between frames, enabling the measurement of multiple myofibrils in one imaging chamber. Because it takes 30 min to accurately measure the proportion of SRX, multiplexing offers a means to accelerate data collection, rather than observing myofibrils in series. Here we show that mavacamten nearly eliminates the DRX phase and that deoxyATP reduces the contribution of the SRX phase, providing the upper and lower bounds of the response. We have presented this technique to enable future studies using any myofibril source, including those containing mutations isolated from patients or stem cell derived, or to test for other compounds that alter the DRX/SRX ratio. Such studies may begin to shed light on perhaps the most pressing question, which is how the DRX/SRX ratio is maintained and modulated. Rapid interchange between DRX and SRX would result in a single phase, therefore two states are being maintained in the relaxed condition. Previous studies have shown that mavacamten inhibition has a lower K_i in HMM (a two-headed myosin construct) than with S1 alone, indicating that myosin's structure itself contributes to inhibition. Furthermore, two phases are seen in myofibrils versus a single phase in purified myosin (Walklate et al. 2022; Mohran et al. 2024), this suggests that interactions with other proteins in the thick filament may also affect myosin's activity. Structural studies in the absence of stabilising treatments reveal such interactions may come from titin and cMyBP-C in the thick filament (Chen et al. 2024). These proteins are the likely conduits of DRX/SRX ratio modulation due to factors such as load and phosphorylation. Together, these observations point towards both the structure of myosin, and interactions with components of the thick filament contributing to modulation of the DRX/SRX ratio.

Although we have demonstrated a simple, rapid tool to measure and quantify myosin activity in a near-native environment, other methods offer their own valuable insights such as polarization, FRET, SHG and X-ray diffraction that measure the physical positions of the heads (Nucciotti et al. 2010; Kampourakis and Irving 2015; Fusi et al. 2016; Irving and Craig 2019; Chu et al. 2021; Ma et al. 2022; Rasicci et al. 2022; Brunello and Fusi 2024), which may relate to myosin's biochemical states. Nonetheless, directly imaging fluorescent ATP release from myofibrils adds significantly to the tools that can be used to fully solve the origin of the paradox of energy usage in the heart and other muscle tissues.

Methods

No live animals were used in this study. Muscle tissue was collected in accordance with the U.K. Animals (Scientific Procedures) Act 1986 and associated guidelines.

Dissection and storage of Porcine heart

The heart of a freshly euthanised adult farm pig was submerged in ice-cold cardioplegic solution (5.5 mM Glucose, 0.5 mM $MgSO_4$, 24 mM KCl, 20 mM $NaHCO_3$, 109 mM NaCl, 0.9 mM H_2NaO_4P, 1.8 mM $CaCl_2$, 0.01% (w/v) NaN_3, pH 7.4) immediately after excision. Whilst submerged, left ventricular trabecular samples were dissected and, cut into ~5 mm thick pieces, individually wrapped in foil, immediately flash frozen and stored long-term at −80 °C.

Myofibril isolation

Porcine left ventricular trabecular myofibril suspensions were prepared as follows: a flash-frozen sample of porcine left ventricular trabeculae was rapidly thawed in chilled Prep buffer (20 mM MOPS, 132 mM NaCl, 5 mM KCl, 4 mM $MgCl_2$, 5 mM EGTA, 0.01% (w/v) NaN_3, 5 mM DTT, protease inhibitor cocktail (A32965; Thermo Scientific), pH 7.1 at RT) (Vikhorev, Ferenczi, and Marston 2016) and cut into ~1 mm thick strips. Sample strips were transferred to 500 µl of Prep buffer in a 2 ml microcentrifuge tube for homogenization using a Tissue Ruptor II (Qiagen) at medium-low speed for 10 s twice, with a 1-minute rest on ice between. Homogenized tissue was then permeabilized for 30 min at 4 °C, rotating, in Permeabilization buffer (Prep buffer + 1% Triton X-100). Myofibrils were collected by centrifugation at 1000 g for 3 min and resuspended in chilled Prep buffer. Washes were repeated 3 times to remove all traces of Triton X-100 and myofibril suspensions were diluted or concentrated where necessary to obtain an OD_{600}

of ~0.6. Myofibril suspensions were stored at 4 °C and discarded at the end of each day.

Microfluidic flowcells

Microfluidic flowcells were constructed by adhering a plasma-cleaned borosilicate coverslip (Menzel Gläser, 24 × 40 mm, 1.5 thickness), coated in 5 µg/ml ≥ 300KDa poly-L-lysine (PLL, Sigma) to a standard microscope slide prepared for microfluidics, using a 360 µm thick adhesive gasket. Microscope slides were prepared for microfluidics by drilling two 1.5 mm diameter holes, 1.5 cm apart and adhering polyethylene tubing (Gradko, GE-0086-033, 0.86 mm internal diameter, 0.33 mm wall) to each using an acrylic bonder (RS, 144–406). Flowcells were connected to a syringe pump (WPI, AL-1000) at one end and at the other, to a 1.5 ml microcentrifuge tube with holes to allow access of pipette tips. 200 µl of myofibril suspension was added to the 1.5 ml microcentrifuge tube and drawn into the flowcell at 1 ml/min then washed back through at 0.2 ml/min. To allow adhesion of myofibrils to the PLL-coated surface, flowcells were incubated on ice for 30 min. Excess non-adherent myofibrils were withdrawn from the flowcell using 600 µl Prep buffer at 10 ml/min.

Image acquisition

All imaging was carried out at room temperature (21 °C) using a custom-built oblique angle fluorescent (OAF) microscope (Desai et al. 2015). The sample was illuminated for 15 ms every 5 s using a 561 nm laser (OBIS LS laser, Coherent, USA) to excite Cy3-ATP, for a total time of 30 min.

Myofibrils were incubated with Cy3-ATP buffer (Prep buffer + 1 µM Cy3-ATP, 500 µM ATP, 0.5 mM phosphoenolpyruvate (PEP), 2.2 units Pyruvate kinase (PK)) for 30 min at RT. Following this, a single frame was taken of the myofibril fully saturated with Cy3-ATP, followed by a rapid wash with Chase buffer (Prep buffer + 5 mM ATP, 5 mM PEP, 22 units PK) at 10 ml/min. To increase efficiency, flowcells were mounted onto a custom-built automated stage programmed to move between user-specified positions along one axis. Between each frame images from neighbouring myofibrils were taken. Use of this automated stage allowed up to 4 myofibrils to be imaged during the 30-minute imaging period.

Mavacamten (MedChemExpress) was solubilized in 100% DMSO and added to the Chase buffer at final concentration of 30 µM with a final DMSO of 0.3% v/v. For 100% dATP experiments, 5 mM dATP (NEB N0440S) was used in the Chase buffer replacing unlabelled ATP.

Data analysis

To extract the rate of fluorescence decay for each myofibril, an ROI was drawn using ImageJ to encompass the entire myofibril and the total intensity profile was extracted through time. These data were transferred to Excel and then fitted to the exponential decays as shown in Fig. 1 to provide both rate constants and amplitudes.

For the Gaussian mixture model, we used Matlab's inbuilt function with diagonal covariance and the number of components fixed at two. The mixtures calculation was iterated 1000 times for best fit and then repeated 100 times to determine the distribution of best fit means and standard deviations for DRX and SRX. These values were then used to calculate the boundaries between DRX and SRX by altering the multiple of standard deviations that led to an equal population of DRX and SRX.

Author contributions MP & AN conducted the experiments, MP, NMK & AN analysed the results, KSC, TK, MAG, NMK conceived the experiments, NMK wrote the manuscript with assistance from all authors, who also reviewed the manuscript. NMK sought funding and supervised the development and outputs of the project.

Data availability No datasets were generated or analysed during the current study.

Declarations

Competing interests The authors declare no competing interests.

References

Amrute-Nayak M, Lambeck K-A, Radocaj A, Huhnt HE, Scholz T, Hahn N, Tsiavaliaris G, Walter WJ, Brenner B (2014) ATP turnover by individual myosin molecules hints at two conformers of the myosin active site. Proc Natl Acad Sci U S A 111:2536–2541

Anderson RL, Trivedi DV, Sarkar SS, Henze M, Ma W, Gong H, Rogers CS, Gorham JM, Wong FL, Morck MM, Seidman JG, Ruppel KM, Irving TC, Cooke R, Green EM, Spudich JA (2018) Deciphering the super relaxed state of human beta-cardiac myosin and the mode of action of Mavacamten from myosin molecules to muscle fibers. Proc Natl Acad Sci U S A 115:E8143–E8152

Brunello E, Fusi L (2024) Regulating striated muscle contraction: through thick and thin. Annu Rev Physiol 86:255–275
Cail RC, Baez-Cruz FA, Winkelmann DA, Goldman YE, Ostap EM (2025) Dynamics of beta-cardiac myosin between the super-relaxed and disordered-relaxed states. J Biol Chem 301:108412
Chen L, Liu J, Rastegarpouyani H, Janssen PML, Pinto JR, Taylor KA (2024) Structure of mavacamten-free human cardiac thick filaments within the sarcomere by cryoelectron tomography. Proc Natl Acad Sci U S A 121:e2311883121
Chu S, Muretta JM, Thomas DD (2021) Direct detection of the myosin super-relaxed state and interacting-heads motif in solution. J Biol Chem 297:101157
Conibear PB, Geeves MA (1998) Cooperativity between the two heads of rabbit skeletal muscle heavy meromyosin in binding to actin. Biophys J 75:926–937
Conibear PB, Jeffreys DS, Seehra CK, Eaton RJ, Bagshaw CR (1996) Kinetic and spectroscopic characterization of fluorescent ribose-modified ATP analogs upon interaction with skeletal muscle myosin subfragment 1. Biochemistry 35:2299–2308
Cooke R (2011) The role of the myosin ATPase activity in adaptive thermogenesis by skeletal muscle. Biophys Rev 3:33–45
Craig R, Padron R (2022) Structural basis of the super- and hyper-relaxed states of myosin II. J Gen Physiol. https://doi.org/10.1085/jgp.202113012
Cremo CR, Neuron JM, Yount RG (1990) Interaction of myosin subfragment 1 with fluorescent ribose-modified nucleotides. A comparison of vanadate trapping and SH1-SH2 cross-linking. Biochemistry 29:3309–3319
Desai R, Geeves MA, Kad NM (2015) Using fluorescent myosin to directly visualize cooperative activation of thin filaments. J Biol Chem 290:1915–1925
Ferenczi MA, Homsher E, Simmons RM, Trentham DR (1978) Reaction mechanism of the magnesium ion-dependent adenosine triphosphatase of frog muscle myosin and subfragment 1. Biochem J 171:165–175
Fraser ID, Marston SB (1995) In vitro motility analysis of actin-tropomyosin regulation by troponin and calcium. The thin filament is switched as a single cooperative unit. J Biol Chem 270:7836–7841
Fusi L, Brunello E, Yan Z, Irving M (2016) Thick filament mechano-sensing is a calcium-independent regulatory mechanism in skeletal muscle. Nat Commun 7:13281
Gollapudi SK, Yu M, Gan QF, Nag S (2021) Synthetic thick filaments: a new avenue for better understanding the myosin super-relaxed state in healthy, diseased, and mavacamten-treated cardiac systems. J Biol Chem 296:100114
Gordon AM, Homsher E, Regnier M (2000) Regulation of contraction in striated muscle. Physiol Rev 80:853–924
Hiratsuka T (1983) New ribose-modified fluorescent analogs of adenine and guanine nucleotides available as substrates for various enzymes. Biochim Biophys Acta 742:496–508
Hooijman P, Stewart MA, Cooke R (2011) A new state of cardiac myosin with very slow ATP turnover: a potential cardioprotective mechanism in the heart. Biophys J 100:1969–1976
Irving TC, Craig R (2019) Getting into the thick (and thin) of it. J Gen Physiol 151:610–613
Kampourakis T, Irving M (2015) Phosphorylation of myosin regulatory light chain controls myosin head conformation in cardiac muscle. J Mol Cell Cardiol 85:199–206
Lymn RW, Taylor EW (1971) Mechanism of adenosine triphosphate hydrolysis by actomyosin. Biochemistry 10:4617–4624
Ma W, Nag S, Gong H, Qi L, Irving TC (2022) Cardiac myosin filaments are directly regulated by calcium. J Gen Physiol. https://doi.org/10.1085/jgp.202213213
McKillop DF, Geeves MA (1993) Regulation of the interaction between actin and myosin subfragment 1: evidence for three states of the thin filament. Biophys J 65:693–701
Mohran S, Kooiker K, Mahoney-Schaefer M, Mandrycky C, Kao K, Tu AY, Freeman J, Moussavi-Harami F, Geeves M, Regnier M (2024) The biochemically defined super relaxed state of myosin-A paradox. J Biol Chem 300:105565
Mohran S, Kooiker KB, Naim A, Pilagov M, Asencio A, Turner KL, Ma W, Flint G, Jiang S, Zhao J, McMillen TS, Mandrycky C, Mahoney-Schaefer M, Irving TC, Tanner BCW, Kad NM, Regnier M, Moussavi-Harami F (2025) Myosin modulator aficamten inhibits force in cardiac muscle by altering myosin's biochemical activity without changing thick filament structure. bioRxiv. https://doi.org/10.1101/2025.05.14.654110
Myburgh KH, Franks-Skiba K, Cooke R (1995) Nucleotide turnover rate measured in fully relaxed rabbit skeletal muscle myofibrils. J Gen Physiol 106:957–973
Nelson SR, Li A, Beck-Previs S, Kennedy GG, Warshaw DM (2020) Imaging ATP consumption in resting skeletal muscle: one molecule at a time. Biophys J 119:1050–1055
Nucciotti V, Stringari C, Sacconi L, Vanzi F, Fusi L, Linari M, Piazzesi G, Lombardi V, Pavone FS (2010) Probing myosin structural conformation *in vivo* by second-harmonic generation microscopy. Proc Natl Acad Sci U S A 107:7763–7768
Pilagov M, Heling L, Walklate J, Geeves MA, Kad NM (2023) Single-molecule imaging reveals how Mavacamten and PKA modulate ATP turnover in skeletal muscle myofibrils. J Gen Physiol. https://doi.org/10.1085/jgp.202213087
Pilagov M, Steczina S, Naim A, Regnier M, Geeves MA, Kad NM (2025) Spatially resolving how phosphorylation affects ß-cardiac myosin activity in Porcine myofibril sarcomeres with single molecule resolution. bioRxiv.2024.2006.2027.600847. Spatially resolving how cMyBP-C phosphorylation and haploinsufficiency in porcine and human myofibrils affect β-cardiac myosin activity.J Gen Physiol. 157(5):e202413628. https://doi.org/10.1085/jgp.202413628
Poole KJ, Lorenz M, Evans G, Rosenbaum G, Pirani A, Craig R, Tobacman LS, Lehman W, Holmes KC (2006) A comparison of muscle thin filament models obtained from electron microscopy reconstructions and low-angle X-ray fibre diagrams from non-overlap muscle. J Struct Biol 155:273–284
Rasicci DV, Tiwari P, Bodt SML, Desetty R, Sadler FR, Sivaramakrishnan S, Craig R, Yengo CM (2022) Dilated cardiomyopathy mutation E525K in human beta-cardiac myosin stabilizes the interacting-heads motif and super-relaxed state of myosin. Elife. https://doi.org/10.7554/eLife.77415
Regnier M, Rivera AJ, Chen Y, Chase PB (2000) 2-deoxy-ATP enhances contractility of rat cardiac muscle. Circ Res 86:1211–1217
Solzin J, Iorga B, Sierakowski E, Gomez Alcazar DP, Ruess DF, Kubacki T, Zittrich S, Blaudeck N, Pfitzer G, Stehle R (2007) Kinetic mechanism of the Ca2+-dependent switch-on and switch-off of cardiac troponin in myofibrils. Biophys J 93:3917–3931
Spudich JA (2019) Three perspectives on the molecular basis of hypercontractility caused by hypertrophic cardiomyopathy mutations. Pflugers Arch 471:701–717
Starr R, Offer G (1978) The interaction of C-protein with heavy meromyosin and subfragment-2. Biochem J 171:813–816
Stehle R, Solzin J, Iorga B, Poggesi C (2009) Insights into the kinetics of Ca2+-regulated contraction and relaxation from myofibril studies. Pflugers Arch 458:337–357
Stewart MA, Franks-Skiba K, Chen S, Cooke R (2010) Myosin ATP turnover rate is a mechanism involved in thermogenesis in resting skeletal muscle fibers. Proc Natl Acad Sci U S A 107:430–435
Toseland CP, Webb MR (2011) Fluorescent nucleoside triphosphates for single-molecule enzymology. Methods Mol Biol 778:161–174
Ušaj M, Moretto L, Vemula V, Salhotra A, Månsson A (2021) Single molecule turnover of fluorescent ATP by myosin and actomyosin unveil elusive enzymatic mechanisms. Commun Biol 4:64

Walklate J, Kao K, Regnier M, Geeves MA (2022) Exploring the super-relaxed state of myosin in myofibrils from fast-twitch, slow-twitch, and cardiac muscle. J Biol Chem 298:101640

Woodward SK, Eccleston JF, Geeves MA (1991) Kinetics of the interaction of 2‘(3’)-O-(N-methylanthraniloyl)-ATP with myosin subfragment 1 and actomyosin subfragment 1: characterization of two acto-S1-ADP complexes. Biochemistry 30:422–430

Zampieri M, Argiro A, Marchi A, Berteotti M, Targetti M, Fornaro A, Tomberli A, Stefano P, Marchionni N, Olivotto I (2021) Mavacamten, a novel therapeutic strategy for obstructive hypertrophic cardiomyopathy. Curr Cardiol Rep 23:79

Vikhorev PG, Ferenczi MA, Marston SB (2016) Instrumentation to study myofibril mechanics from static to artificial simulations of cardiac cycle. MethodsX3:156-70. https://doi.org/10.1016/j.mex.2016.02.006